THE JOURNAL OF PHYSICAL CHEMISTRY C

ARTICLE

pubs.acs.org/JPCC

Density Functional/All-Electron Basis Set Slab Model Calculations of the Adsorption/Dissociation Mechanisms of Water on α-Al_2O_3(0001) Surface

Baoshan Wang,*[,†] Hua Hou,[†] Yunbai Luo,[†] Yan Li,[‡] Yuming Zhao,[‡] and Xiaolin Li[‡]

[†]College of Chemistry and Molecular Sciences, Wuhan University, Wuhan, 430072, People's Republic of China

[‡]Electric Power Research Institute, China Southern Grid, Guangzhou, 510623, People's Republic of China

Supporting Information

ABSTRACT: The microscopic reaction mechanism for the water adsorption/dissociation processes on the α-Al_2O_3(0001) surface was calculated using density functional theory with the *all-electron* triple numerical polarized basis sets. Both unit-cell and 2 × 2 supercell slab models were employed to investigate the coverage-dependent hydroxylation of the surface. Geometries of the molecular adsorbed intermediates, transition states, and the hydroxylated products were fully optimized, and the energetic reaction routes were clarified. The hydroxylation occurs predominantly via the low-barrier 1,4-hydrogen migration path, and the 1,2-dissociation path is competitive. The 1,2-hydroxylated surface is more preferable thermodynamically in the consideration of reaction exothermicity. It was found that the in-plane hydrogen atoms can roam between the surface oxygen atoms, resulting in isomerization between the 1,2- and 1,4-hydroxylated products. Calculations for the multiple layer adsorption confirm that the hydroxylated surface is relatively inert to further hydroxylation by water. Further added water molecules prefer to form multilayered hexagonal ice-like arrangements through a hydrogen-bonding network. The electric field might not play a significant role in either surface reconstruction or the hydroxylation process until it exceeds 10^8 V/m. The present theoretical work is useful to gain some new insights on the ice accumulation of high-voltage power lines under high humidity and supercooled environment.

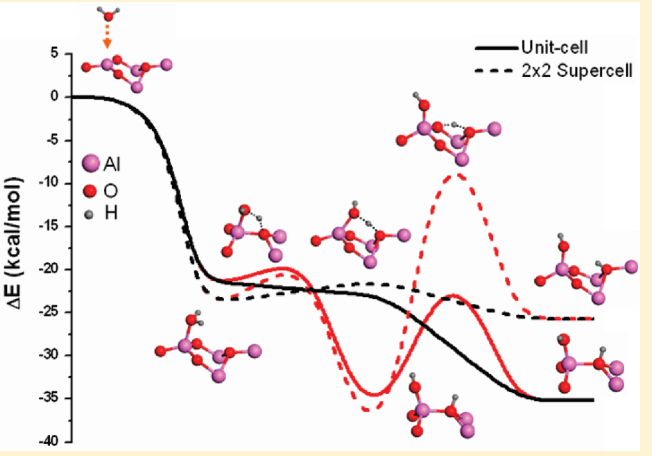

1. INTRODUCTION

The interaction between H_2O molecules and the α-Al_2O_3(0001) surface has attracted considerable attention both experimentally and theoretically. Alumina is one of the most important materials and is widely used in electronics, catalysis, and environmental chemistry. We are interested in the water adsorption/dissociation on the Al_2O_3 surface because it is a key process involved in the icing of high-voltage power lines.[1] It is well-known that ice accumulation creates significant problems. A successful method or composition for inhibiting surface icing relies on the full understanding of the microscopic mechanics of water adsorption and/or decomposition on the aluminum oxide surfaces.

Numerous investigations have focused on the hydroxylation and dehydroxylation of the alumina surface in the presence of water. Mechanically, it is currently accepted that water dissociates on the Al-terminated Al_2O_3(0001) surface, in particular at surface defect sites, as concluded from high-resolution electron-energy-loss spectroscopy, vibrational spectroscopy, LEED, thermal and laser-induced desorption, AFM, and dynamic-mode SFM.[2−7] Using surface-sensitive X-ray photoemission experiments, Eng and co-workers investigated experimentally the surface properties of the hydrated α-Al_2O_3(0001) surface and reported an oxygen-terminated surface coupled with the formation of an ordered contact water layer.[8] The hydroxyl desorption energies were measured in the range from 23 to 41 kcal/mol.[5] Moreover, it is found that the adsorption/dissociation depends strongly on water coverage and preparative conditions.[9]

Theoretically, the dissociative adsorption mechanism of water at the Al_2O_3(0001) surface has been calculated extensively using various cluster/lattice models and first-principles methodologies.[10−16] While most of these studies focused on the calculations of the adsorption structures and energies of the hyoxylated alumina surface, there are some investigations on the detailed molecular mechanisms. Wittbrodt, Hase, and Schlegel employed several Al_nO_m cluster models to calculate the adsorption/dissociation

Received: April 18, 2011
Revised: May 30, 2011
Published: June 01, 2011

Table 1. Geometric and Energetic Changes from Al_2O_3 Bulk to the (0001) Surface Calculated at Various Levels of Theory[a]

basis set	DND	DND	DND	DND	DND	DND	TNP	TNP	TNP	TNP
k-points	Γ[b]	Γ[c]	Γ	2 × 2 × 1	3 × 3 × 1	3 × 3 × 3	Γ	3 × 3 × 3	5 × 5 × 5	7 × 7 × 7
$\delta(d_{Al-O})$[d]	−0.64	−0.62	−0.60	−0.62	−0.62	−0.62	−0.61	−0.62	−0.62	−0.62
$\delta(l_{Al-O})$[e]	−0.17	−0.15	−0.15	−0.15	−0.15	−0.15	−0.16	−0.16	−0.16	−0.16
$\delta(\varphi_{AlO_3})$[f]	+53	+51	+49	+51	+51	+51	+50	+51	+51	+51
SE[g]	1.56	1.63	1.65	1.63	1.62	1.63	1.53	1.52	1.52	1.52

[a] The experimental unit-cell lattice constants are employed unless stated otherwise. [b] Optimized lattice parameters. [c] The 2 × 2 supercell model. [d] Interlayer spacing between the outmost Al and O layers, in angstroms. [e] Al−O bond distance, in angstroms. [f] Dihedral angle of the AlO_3 tetrahedral structure, in degrees. [g] Surface energy in J/m^2, SE = $(E_{surface} - E_{bulk})/2A$, where A is the basal surface area.

routes at the B3LYP/6-31+G* level of theory.[17] It was found that the reaction takes place with the formation of the molecular adsorption intermediates and follows two distinct dissociation paths, namely, 1,2 migration (proton transfer to the nearest crystal oxygen) and 1,4-H migration (proton transfer to the second nearest oxygen). The barrier to 1,4 dissociation is 5−7 kcal/mol higher than the 1,2 barrier and 1,2 dissociation of water is more exothermic than the 1,4 process by ca. 5 kcal/mol. However, the periodic ab initio molecular dynamics simulation based on the Car−Parrinello methodology performed by Hass, Schneider, Curioni, and Andreoni presented contrary results.[18,19] With a periodic slab, both 1,2- and 1,4-dissociative pathways were investigated using the BLYP functional with the plane wave and pseudopotentials. At low water coverage (e.g., 3 × 3 supercell), it was found that the free energy barriers for 1,2 and 1,4-H migrations are 6.6 and 2.2 kcal/mol, respectively. Evidently, the 1,4 dissociation is strongly favored kinetically over 1,2 dissociation. More recently, Ranea, Carmichael, and Schneider investigated the intermediate steps in the hydrolysis of Al_2O_3(0001) using the plane-wave density functional theory (PW91) with the projector augmented wave (PAW) approach for describing electronic core states.[19] With the 2 × 2 supercell model, the transition state for the 1,2-dissociation pathway of a single water molecule was located using the climbing image nudged elastic band (CI-NEB) method. The barrier to 1,2 dissociation is 4.4 kcal/mol with respect to the initial molecular absorption intermediate. The 1,4-dissociation path was not yet studied.

In this work we have attempted to clarify two questions. First is the electronic structures of all the stationary points along the reaction coordinates for the water adsorption/dissociation on the Al_2O_3(0001) surface. Both 1,2- and 1,4-dissociation paths and the subsequent isomerization paths of their products will be explored. Density functional theory with the all-electron basis sets is used for this purpose, in contrast with the previous plane-wave and pseudopotential schemes. The second question is the dependence of the reaction mechanism upon the external environments, including water coverage (humidity), temperature (0−1000 K), and electric fields (10^5−10^{10} V/m, of particular importance for high-voltage power lines). Both unit-cell (monolayer, ML = 1) and 2 × 2 supercell (ML = 0.25) models have been used for this purpose. Moreover, multiple-layer water adsorption for the unit cell has been studied as well.

2. COMPUTATIONAL METHODS

First-principles total energy calculations were carried out with the density functional theory (DFT) using the Dmol^3 program.[21] Electron exchange and correlation energies were calculated within the generalized gradient approximation (GGA) using Becke−Lee−Yang−Parr (BLYP).[22−24] Rather than the analytic Gaussian-type basis sets, the all-electron numerical basis functions, which are generated as values on an atomic-centered spherical-polar mesh, were employed herein. The numerical part is obtained by numerically solving the atomic DFT equations. It has been shown that within the DFT context the numerical basis set is capable of minimizing or even eliminating basis set superposition error (BSSE).[25] This is particularly useful for the chemical reaction (intermediates, transition state, and isolated reactants and products) and hydrogen-bonding calculations of our concern. Double numerical (DND) and triple numerical polarized (TNP) basis sets were used in this study. DND basis sets include a d-type polarization function on heavy atoms, while the TNP basis sets include additional sets of d-type polarization functions on all atoms. It was previously shown that an all-electron basis set with the addition of d functions is essential for a proper description of high-valence Al atoms.[26,27]

The atom-centered grids were used for the numerical integration including about 2000 grid points for each atom and with a real-space cutoff of 4.8 Å. Self-consistent-field (SCF) convergence criterion was set to the root-mean-square change in the electronic density to be less than 10^{-6} eV. It is noted that a thermal smearing of 0.005 au has been applied to the orbital occupation to speed up convergence.

The equilibrium geometries of reactants, intermediates, and products were fully optimized using the Broyden−Fletcher−Goldfarb−Shanno (BFGS) method within the delocalized coordinates. Transition states were obtained tentatively using the synchronous transit methods and then refined through the eigenvector following optimization. The convergence criteria applied for geometry optimization are enforced to 10^{-5} au for energy, 0.002 au/Å for force, and 0.005 Å for maximum displacement. Harmonic vibrational frequencies of the optimized structures were computed by diagonalizing the mass-weighted second-derivative matrix which was built using two-sided finite differences with a displacement step of 0.01 Å. The minimum has all real frequencies and the transition state has one and only one imaginary frequency along the reaction coordinates. Thermodynamic calculations were performed using the rigid-rotor harmonic oscillator approximations, and the zero-point energies (ZPE) were corrected for all the energies without scaling.

The Al-terminated Al_2O_3(0001) basal surface was built by cleaving the bulk corundum crystal. It consists of an 18-layer-thick slab with six complete AlO_3Al layers ($Al_{12}O_{18}$). To avoid unphysical interlayer interactions, the slabs were separated by a vacuum region of 10 Å. In addition, a 2 × 2 supercell model ($Al_{48}O_{72}$) was considered in this work in order to simulate the low water coverage. It is worth noting that all atoms in the slab are allowed to relax during the optimization without any geometric or symmetrical constraints. To sample the first Brillouin zone of

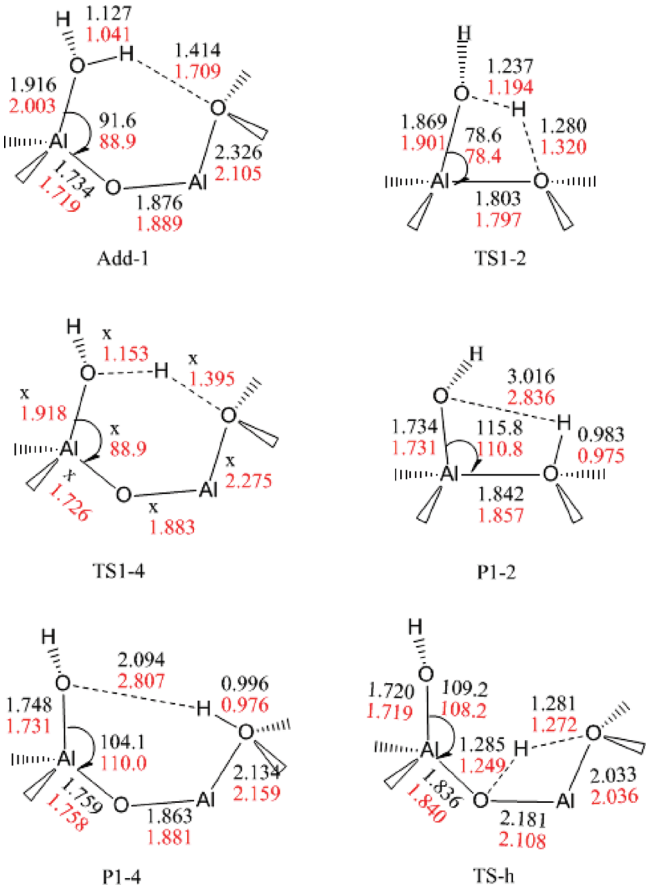

Figure 1. Optimized geometries of adsorbed molecular intermediate Add-1, transition states for 1,2 (TS1-2) and 1,4 (TS1-4) dissociation paths, and the corresponding products P1-2 and P1-4. TS-h represents the transition state for the surface hydrogen isomerization path connecting P1-2 and P1-4. Only the key structures taken from the unit-cell slab models are shown for clarity. Bond distances are in angstroms, and angles are in degrees. First entries (in black): BLYP/DND with only Γ-point sampling. Second entries (in red): BLYP/TNP with 3 × 3 × 3 *k*-points sampling.

the hexagonal lattice correctly, various Γ-centered meshes have been carefully tested for convergence using a range of *k*-points up to 9 × 9 × 9 (365 irreducible *k*-points).

3. RESULTS AND DISCUSSION

3.A. Al_2O_3(0001) Surface Energies. Although the BLYP method within the plane wave and pseudopotential basis has been successfully used in the calculations of various metal oxides, it is worth examining its performance for the present system because we employed all-electron numerical basis sets. Moreover, it is essential to test the convergence of both basis set and *k*-point mesh for the slab model calculations. Therefore, the Al_2O_3 bulk and the basal (0001) surface were first investigated. The geometric changes from bulk to surface and the surface energies were obtained as a function of *k*-points and basis sets. The results are summarized in Table 1 for comparison.

The BLYP/DND with only Γ-point optimized lattice constants of bulk Al_2O_3 are a = 4.816 Å and c = 13.187 Å, which are larger than those of the experimental cell by 1.2 and 1.5%, respectively. The surface Al atom relaxed toward the surface

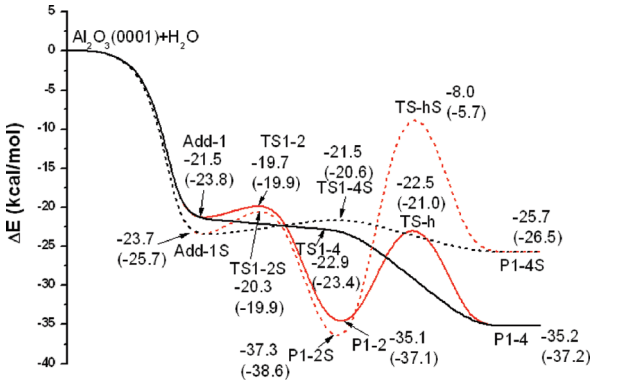

Figure 2. Energetic reaction routes obtained at the BLYP/TNP/3 × 3 × 3 *k*-points level of theory. Both the unit-cell model (solid lines) and the 2 × 2 supercell model (dashed lines) are shown together for comparison. 1,2- and 1,4-dissociation pathways starting from the complexes are shown in red and black, respectively, for clearness. Zero-point energies are included in the relative energies. The uncorrected energies are listed in parentheses.

O atoms, decreasing the interlay spacing from 0.84 to 0.20 Å. The relaxation ratio is 76% in comparison with the experimental data of 51−63%.[28,29] The surface energy is 1.56 J/m^2, which is smaller than the experimental value of 1.69 or 2.04 J/m^2.[30,31] If the experimental lattice constant a = 4.759 Å was used, the relaxation ratio becomes 72% and the surface energy is 1.65 J/m^2. Apparently, the agreement with the experimental data is even better, although the slight change of the lattice constants in the lateral direction does not affect the surface significantly. Note that the geometric reconstruction of the surface could be better characterized using the AlO_3 tetrahedral. As shown in Table 1, the AlO_3 dihedral angle decreases from 104° in the bulk to 157° in the surface. The relaxation ratio is 51%.

As shown in Table 1, both basis sets and *k*-points do affect surface geometry and surface energy more or less. The converged results could be readily obtained using BLYP/TNP with the 3 × 3 × 3 Γ-centered meshes (a total of 14 irreducible *k*-points).

3.B. Single Water Adsorption/Dissociation at Unit Cell. The optimized geometries of the stationary points are shown in Figure 1. The corresponding energetic reaction routes are schematically shown in Figure 2. A single isolated water molecule approaches the surface Al atom to form an intermediate, denoted as Add-1 in Figure 1. Apparently, it includes an intramolecular hydrogen bonding geometry, occurring between one of the hydrogen atoms of water (H_w) and the surface oxygen atom (O_s') with a distance of 1.709 Å. This structure may enhance the stability of the adduct significantly. The distance between the oxygen atom of water (O_w) and the surface Al atom (Al_s) is relatively long, 2.003 Å. Therefore, Add-1 is considered to be a molecular adsorbed complex. The binding energy is 23.8 kcal/mol (21.5 kcal/mol with ZPE correction).

Note that the geometry of Add-1 strongly depends on the theoretical levels of theory. As shown in Table 2, Γ-point sampling tends to give the dissociative structure in view of the short $H_w\cdots O_s$ hydrogen bond. In fact, within TNP/Γ, the optimization of the intermediate leads to the dissociative product directly. In addition, the geometries of other stationary points show a similar dependence on both basis sets and *k*-points, as can be seen in Figure 1. However, the converged results could be obtained at the BLYP/TNP/3 × 3 × 3 level, as concluded from

Table 2. Dependence of the Geometry of the Water Absorbed Intermediate, Add-1, on the Theoretical Levels Employed in the Optimization

basis set	DND	DND	DND	DND	TNP	TNP	TNP
k-points	Γ	3 × 3 × 3	5 × 5 × 5	7 × 7 × 7	3 × 3 × 3	5 × 5 × 5	7 × 7 × 7
O_w-Al_s	1.916	2.018	2.018	2.018	2.003	2.004	2.004
O_w-H_w	1.127	1.041	1.041	1.041	1.039	1.039	1.039
$H_w\cdots O_s'$	1.414	1.746	1.747	1.747	1.709	1.710	1.710
Al_s-O_s	1.734	1.728	1.728	1.728	1.719	1.719	1.719
$Al_s\cdots O_s'$[a]	2.326	2.084	2.084	2.084	2.105	2.105	2.104
E[b]	−0.04830	−0.01843	−0.01865	−0.01865	−0.13826	−0.13880	−0.13882
ΔE[c]	−27.9	−27.2	−27.2	−27.2	−23.8	−23.8	−23.8

[a] Distance of Al_s to the next nearest O_s'. [b] Total electronic energy, in −4343 hartrees. [c] Relative energies to the isolated water and the free (0001) surface, in kcal/mol.

Table 2. The change of total energy is less than 15 meV, and the relative energy remains unchanged.

There are two dissociation pathways starting from the initial molecular adduct, as shown in Figure 2. The first route possesses a four-member-ring transition state, TS1-2. The hydrogen atom migrates from water to the nearest O_s atom to form the hydroxylated product P1-2. In view of the breaking O_w-H_w bond and the forming H_w-O_s bond, TS1-2 exhibits a reactant-like structure, and thus it is an early barrier, being consistent with the high exothermicity of the reaction, −35.1 kcal/mol. The barrier height for TS1-2 is 3.9 kcal/mol. After ZPE correction, the barrier reduces to only 1.8 kcal/mol. The second dissociation path undergoes via a six-member-ring transition state, TS1-4. The hydrogen atom of water migrates to the next nearest O_s' atom. TS1-4 shows an obvious early barrier character, the breaking O_w-H_w bond is elongated only slightly, and the forming H_w-O_s' bond is about 0.4 Å longer than the equilibrium OH bond in the product P1-4. The barrier height was calculated to be 0.9 kcal/mol. With ZPE correction the barrier indeed becomes lower than the initial adduct by about 2 kcal/mol. As mentioned above, TS1-4 does not exist if only Γ-point is sampled in the first Brillouin zone of the unit cell. Apparently, the molecular water adsorption intermediate is a metastable structure. Once formed, it will dissociate spontaneously to form the product P1-4. The overall exothermicity is −35.2 kcal/mol.

It is interesting to compare the imaginary frequencies of TS1-2 (860 cm^{-1}) and TS1-4 (447 cm^{-1}). It indicates that the barrier for 1,2 dissociation is much narrower than that for 1,4 dissociation. As a result, the 1,2-reaction route might involve a more significant quantum tunneling effect, which is able to compensate its slightly higher barrier. Therefore, it is conceivable that 1,2- and 1,4-dissociation paths should be competitive especially at lower temperatures.

It should be noted that P1-2 and P1-4 are only conformers of the hydroxylated surface due to periodic boundary and symmetry, as distinguished by the $H_wO_wAl_sO_s$ dihedral angle. The corresponding torsion potential was calculated, and the results are shown in Figure 3. The torsion barrier located at the zero dihedral angle is about 2 kcal/mol. The torsion potential could be best fit using the following four-term function, viz.

$$V(\theta) = 0.286[1 + cos(\theta - 9.2)] + 0.834[1 + cos(2\theta - 4.5)] - 0.147[1 - cos(3\theta + 10.1)] - 0.039[1 - cos(4\theta - 9.1)]$$

This torsion potential might play an important role in the determination of adsorbed water structure on the Al_2O_3 surface.

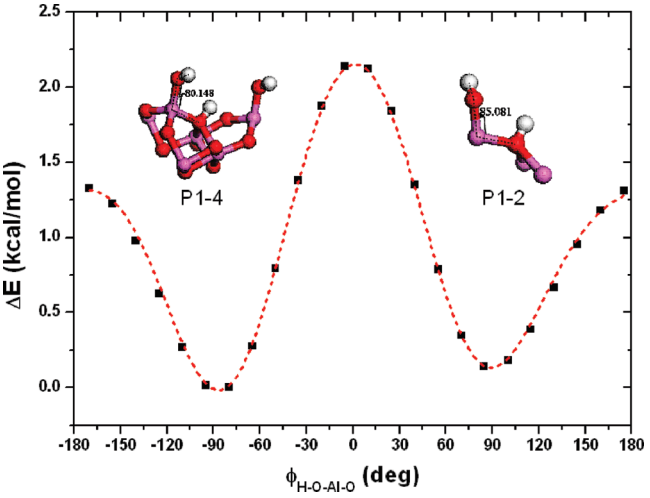

Figure 3. Torsion potential for the hydroxylated surface products (P1-2 and P1-4) around the HOAlO dihedral angles calculated at the BLYP/TNP/3 × 3 × 3 *k*-points level of theory. Dashed line: best-fit four-term torsion potential function. See text for details.

We are currently incorporating it into the force field for large-scale molecular dynamics simulations. The results will be reported elsewhere.

Furthermore, it was found that there is a reactive isomerization path between P1-2 and P1-4. The surface hydrogen atom (H_s) migrates between two surface O_s atoms. The corresponding transition state is denoted as TS-h, as shown in Figure 1. The two reacting H_s-O_s bonds are nearly equal in distance. The barrier height is 12.6 kcal/mol with respect to P1-2. Although TS-h is significantly higher than the torsion barrier, it is still well below the initial water adsorption adduct. Moreover, TS-h involves a large imaginary frequency, 1354 cm^{-1}. Therefore, the surface H_s atoms are capable of roaming between surface O_s atoms on the hydroxylated surface. Experimental observation of such dynamic behavior should be very interesting.

It is desirable to illustrate the structural and atomic charge changes from the Al_2O_3 bulk to the surface, to the water adduct, and to the hydroxylated surface. The atomic Mulliken charges are schematically shown in Figure 4 for all four reaction stages. In the bulk crystal the charges of Al and O are +1.092*e* and −0.702*e*, respectively. For the relaxed (0001) surface, the outmost Al atom becomes more positively charged and the outmost O atoms become more negatively charged, that is, +1.230*e* and −0.942*e*,

Atoms	Bulk	(0001)	Add-1	P1-4
H			+0.374	+0.321
O			−0.770	−0.959
H			+0.223	+0.275
Al	+1.092	+1.230	+1.373	+1.240
O	−0.702	−0.942	−1.024	−0.684
O		−0.944	−0.814	−0.855
O		−0.957	−0.864	−0.861
Al Al		+1.305	+1.250	+1.202
Al		+1.285	+1.238	+1.263
O O O		−0.700 −0.710 −0.756	−0.711 −0.701 −0.711	−0.701 −0.726 −0.672
Al		+1.091	+1.078	+1.085
Al Al		+1.134	+1.118	+1.120
O O O		−0.697 −0.703 −0.758	−0.707 −0.729 −0.720	−0.705 −0.732 −0.722
Al		+1.122	+1.115	+1.111

Figure 4. Mulliken charge distribution for bulk, free surface, adsorption intermediate (Add-1), and the hydroxylated products (P1-4) calculated at the BLYP/TNP/3 × 3 × 3 *k*-points level of theory. The Al interlayer distances are labeled as d_1-d_5 from top to bottom.

respectively. This implies an electron withdrawing from Al to O during the surface reconstruction. Moreover, the charge transfer occurs for the next two layers of O and Al as well. The band gaps for the bulk Al_2O_3 and the (0001) surface were calculated to be 6.8 and 4.6 eV, respectively. Obviously, the (0001) surface is more metallic and thus more reactive.

In view of the initial water adduct, the charge of the O_w atom is −0.770*e*, in comparison with −0.509*e* in the isolated water molecule. With the formation of the O_w-Al_s bond, the surface Al_s atom becomes more positively charged, i.e., +1.373*e*. Meanwhile, the nearest O_s layers become slightly more negatively charged. The next two Al layers are less positive because of the electron withdrawing from the O layers. While the reaction proceeds to the final product, electron redistribution makes the surface Als atom less positively charged, +1.240*e*, comparable to that in the free surface. The formation of a surface HO_s bond leads the O_s atomic charge to be −0.684*e*, close to that in the bulk.

The geometry change including the distances between the first six Al layers, d_1-d_5, as indicated in Figure 4, is listed in Table 3. From bulk to the free surface, the distance between the first two layers, d_1, is significantly contracted from 1.68 Å to 1.12 Å (33%). The distance between the second and the third Al layers (d_2) is contracted by 44%. In contrast, the distance d_3 between the third and fourth Al layers increases by 0.22 Å. The contraction of the further inner layer distances d_4 and d_5 is only marginal. Therefore, the surface reconstruction affects the lattice up to the sixth Al layer.

As for the molecular adsorption complex, although the O_w-Al_s bond is relatively long (∼2.0 Å), water adsorption draws up the surface Al_s atom, as shown by the distance d_1 increasing from 1.12 to 1.36 Å. The tetrahedral angle AlO_3 decreases from 155 to 133°. Once the Al_s-O_wH structure is formed in the product P1-4, the O_w-Al_s distance decreases to

Table 3. Geometric Change (Distances between Al Layers d_1-d_5, in Å, and the AlO_3 Tetrahedral Angle, in deg) along the Reaction Coordinates

stage	bulk	free surface	Add-1	P1-4
d_1	1.68	1.12	1.36	1.62
d_2	0.49	0.28	0.30	0.34
d_3	1.68	1.90	1.85	1.80
d_4	0.49	0.46	0.49	0.50
d_5	1.68	1.70	1.70	1.69
AlO_3	104	155	133	110

1.731 Å. The surface Al_s is pulled onward further, as indicated by the d_1 distance of 1.62 Å, which is very close to that in the bulk. Moreover, the AlO_4 tetrahedral geometry is very close to that in the bulk, e.g., 110° vs 104°.

The above geometric feature and charge distributions suggest that the hydroxylated basal surface of alumina is very stable and the surface Al_s atoms act like those in the bulk crystal. As a result, further addition of water molecules to the surface hydroxylated Al_s should be unfavorable. This speculation has been addressed through examining the multiple-layer water adsorption processes (see section 3.E).

The temperature-dependent Gibbs free energies (ΔG, relative to the initial molecular adduct) of TS1-2, TS1-4, TS-h, P1-2, and P-14 are shown in Figure 5. The dissociation rate constants for 1,2 and 1,4 reactions were estimated using the transition state theory as follows:[46]

$$k(T) = \kappa \frac{k_B T}{h} e^{-\Delta G^{\ddagger}/RT}$$

where κ is the tunneling factor evaluated using the one-dimensional unsymmetrical Eckart potential with the imaginary frequency.[32] k_B and h are the Boltzmann constant and Planck's constant, respectively.

As shown in Figure 5, the free energies for 1,2 and 1,4 barriers increase as the temperatures increase while TS-h and the two products show negative temperature dependence. At temperatures above 500 K, the free energies for 1,4 reaction becomes positive. Apparently, entropy plays an important role in the hydrolysis reactions. In view of the rate constants, the 1,4-decomposition channel exhibits negative temperature dependence because it is an essentially barrier-free process, whereas the 1,2-decomposition channel shows positive dependence. In the whole range of temperatures of interest, the 1,4 mechanism is always dominant. Be aware that the rate constants in Figure 5 are only qualitatively meaningful because of the classical and nonvariational treatment.

3.C. Single Water Adsorption/Dissociation at 2 × 2 Supercell. In order to investigate the coverage dependence of the hydrolysis reaction of the Al_2O_3(0001) surface, a 2 × 2 supercell model, corresponding to the coverage ML = 1/4, was built and the adsorption/dissociation pathways were explored. The geometries of all the stationary points are shown in Figure 6, and the energetic reaction routes are shown in Figure 2 in comparison with the unit-cell model.

In view of the geometric parameters of transition states and products, *k*-point mesh and basis sets have less significance for the 2 × 2 supercell model than that for the unit-cell case. However, the initial adduct, Add-1S, is an exception. As can be seen in Figure 6, at the BLYP/DND level with only Γ-point,

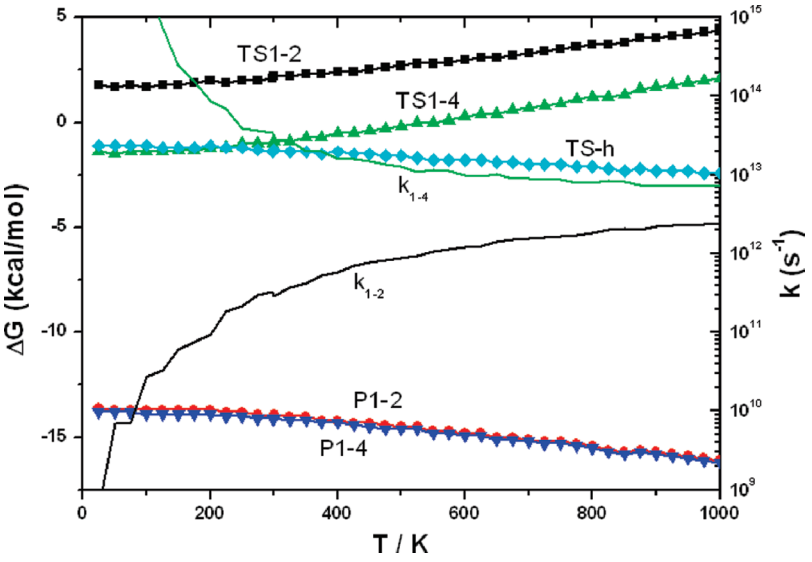

Figure 5. Gibbs free energies (solid lines with symbols) relative to the adsorption intermediate of transition states and products involved in the unit-cell model calculated at the BLYP/TNP/3 × 3 × 3 *k*-points level of theory. The decomposition rate constants for 1,2 (k_{1-2}) and 1,4 (k_{1-4}) channels are shown as well (solid lines).

Add-1S possesses an intramolecular hydrogen bonding, analogous to that in the unit-cell model. When the larger TNP basis set and 3 × 3 × 3 *k*-points are employed, the intramolecular bond disappears and the two O_w—H_w bonds of water molecule are nearly parallel to the two Al_s—O_s bonds. The O_w—Al_s bond is slightly shorter than that of the Add-1 in the unit cell. The binding energy is 23.7 kcal/mol with ZPE correction, which is 2.2 kcal/mol higher than that in the unit cell.

The 1—2 hydrogen migration undergoes via transition state TS1-2S. As shown in Figure 6, TS1-2S is an early barrier. The O_w—Al_s bond decreases to 1.888 Å. The breaking O_w—H_w bond and the forming H_w—O_s bond are 1.198 and 1.320 Å, respectively. It is noted that the geometry of TS1-2S is in good agreement with the result obtained by Ranea, Carmichael, and Schneider[20] using the CI-NEB method, for instance, 1.875, 1.195, and 1.312 Å for O_w—Al_s, O_w—H_w, and H_w—O_s bonds, respectively. The barrier height is 5.8 kcal/mol without ZPE correction, in comparison with 4.4 kcal/mol obtained by Ranea, Carmichael, and Schneider. The ZPE-corrected barrier height is 3.4 kcal/mol.

The 1—4 hydrogen migration occurs via transition state TS1-4S. As shown in Figure 6, TS1-4S is a six-member-ring structure and the reacting H_w atom is in the middle of the two reacting O atoms. The barrier height is 2.2 kcal/mol including ZPE, which is 1.2 kcal/mol lower than TS1-2S. It is interesting to note that the imaginary vibration frequency of TS1-4S is 681 cm^{-1}, which is much smaller than that of TS1-2S, i.e., 1020 cm^{-1}. It appears that TS1-2 is a narrower barrier than TS1-4. The imaginary frequency for TS1-2S obtained by Ranea, Carmichael, and Schneider is 854 cm^{-1}, which is about 15% smaller than our value.[20]

The hydroxylated products are denoted as P1-2S and P1-4S in Figure 6. With respect to the initial molecular adduct, the formation of P1-4S is almost a thermoneutral channel while the production of P1-2S is highly exothermic. Overall, the P1-4S channel is exothermic by −25.7 kcal/mol and the P1-2 channel is exothermic by −37.3 kcal/mol. Interestingly, these two values are just in the range of the experimental data, −23 to −41 kcal/mol.[5] P1-4S isomerizes to P1-2S via transition state TS-hS. As shown in

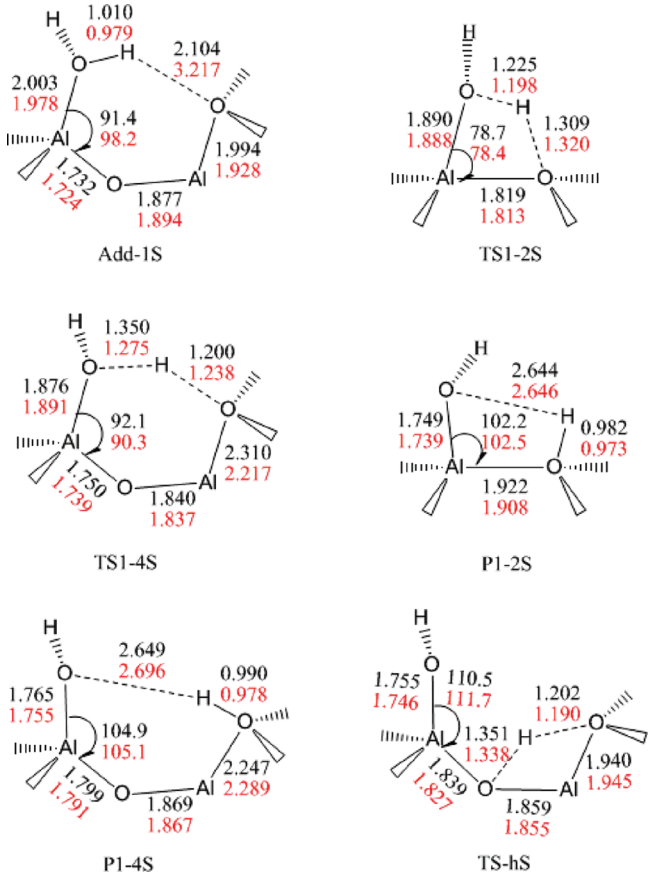

Figure 6. Optimized geometries of adsorbed molecular intermediate Add-1S, transition states for 1,2 (TS1-2S) and 1,4 (TS1-4S) dissociation paths, and the corresponding products P1-2S and P1-4S. TS-hS represents the transition state for the surface hydrogen isomerization path connecting P1-2S and P1-4S. Only the key structures taken from the 2 × 2 supercell slab models are shown for clarity. Bond distances are in angstroms, and angles are in degrees. First entries (in black): BLYP/DND with only Γ-point sampling. Second entries (in red): BLYP/TNP with 3 × 3 × 3 *k*-points sampling.

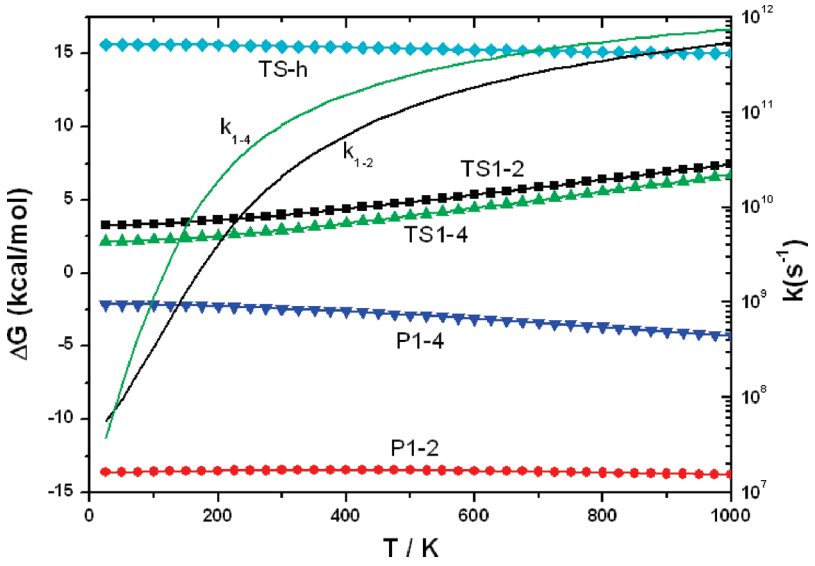

Figure 7. Gibbs free energies (solid lines with symbols) relative to the adsorption intermediate of transition states and products involved in the 2 × 2 supercell slab model calculated at the BLYP/TNP/3 × 3 × 3 *k*-points level of theory. The decomposition rate constants for 1,2 (k_{1-2}) and 1,4 (k_{1-4}) channels are shown as well (solid lines).

Figure 6, TS-hS is more like P1-4S, consistent with the reaction exothermicity. The barrier height is 17.7 kcal/mol relative to P1-4S. However, TS-h is still well below the initial reactants, that is, the isolated water and free basal surface, by about 8 kcal/mol. Therefore, surface hydrogen atom roaming might be able to occur as well.

In comparison with the unit-cell model, the absorption/dissociation of water at lower coverage condition is more exothermic but the barriers for dissociations increase. On the other hand, the barriers to both 1−2 and 1−4 pathways are only marginal compared to the absorption exothermicity. Therefore, the hydroxylation of the $Al_2O_3(0001)$ surface should be fairly feasible even under low humidity environment.

Temperature dependences of the relative Gibbs free energies of various channels are shown in Figure 7, together with the estimated rate constants for 1,2- and 1,4-dissociation channels. Evidently, the 1,2- and 1,4-reaction channels are competitive especially at low temperatures. Both rate constants show positive temperature dependence. The formation of P1-2S from the hydroxylation of the outmost Al_s site and the nearest O_s site is always the most favorable product channel thermodynamically. The other product, P1-4S, may convert to P1-2S rapidly through the surface hydrogen atom roaming process because of the significant extra thermal stability of the latter.

To our knowledge, there is no experimental rate coefficient available to compare with the present theoretical result. For a 3 × 3 supercell model, Hass and co-workers reported the dissociation rate coefficients at 300 K for 1,2- and 1,4-reaction channels to be 10^8 and 1.6×10^{11} s^{-1}, respectively. In comparison with our data of 2.1×10^{10} and 7.4×10^{10} s^{-1} (with Eckart tunneling corrections) for the 2 × 2 supercell modeling, the orders of magnitude for the dominant 1,4-dissociation path are in reasonable agreement.

3.D. Electric Field. At the surface of high-voltage power lines a strong electric field exists. It is interesting to investigate how the electric field affects the surface property and its reactivity. The bulk Al_2O_3 and its (0001) surface were reoptimized within the electric fields ranging from 10^5 to 10^{10} V/m. In principle, there are three types of electric fields, including alternating (ac), positive (+dc), and negative (−dc). Experiments on the ice accumulation on aluminum under supercooled condition shows that ac and +dc fields have similar effects on icing while the −dc fields are unique.[1] Because the high-voltage electric transmission is usually with ac mode in practice, and for simplicity, the electric fields are simulated by applying +dc fields along the +*z* direction, that is, perpendicular to the surface positively.

Total energies of bulk and surface and the outmost Al_sO_s interlayer distances are shown in Figure 8. It is evident that at electric fields lower than 10^8 V/m there is no observable effect on both bulk and surface. For higher electric fields, the energies of bulk and surface decrease but the latter decreases much faster than the former. When the electric fields increase to about 2×10^9 V/m, the $Al_2O_3(0001)$ surface appears to have negative surface energy. Since the surface energy of a solid measures the energy cost of increasing the surface area, if it had been negative, the solid would disintegrate. Therefore, the $Al_2O_3(0001)$ surface becomes metastable under extremely high electric fields. Geometrically, the Al_sO_s interlayer expands suddenly, leading to the bulk-like surface structure; that is, the surface reconstruction might not occur under extremely high electric fields. This phenomenon could be understood in line with the charge distribution of the surface atoms as shown in Figure 4.

Electric fields were then applied to the unit cell to investigate its influence on the surface water adsorption/dissociation reaction. The results are shown in Figure 9. Apparently the surface reactions have not been affected until the electric fields increase to 10^8 V/m. In the presence of electric fields, the barriers to both 1,2- and 1,4-dissociation channels and to the surface hydrogen roaming path are all lowered more or less. Moreover, the hydroxylation products become more exothermic within electric fields. Stan, Tang, Bishop, and Whitesides investigated how the electric fields would affect the nucleation of ice in supercooled water.[33] They found that externally applied electric fields up to 1.6×10^5 V/m do not affect the homogeneous nucleation of ice. Fields in the range of 10^7−10^8 V/m would be required to cause an observable increase in the rate of nucleation. The present

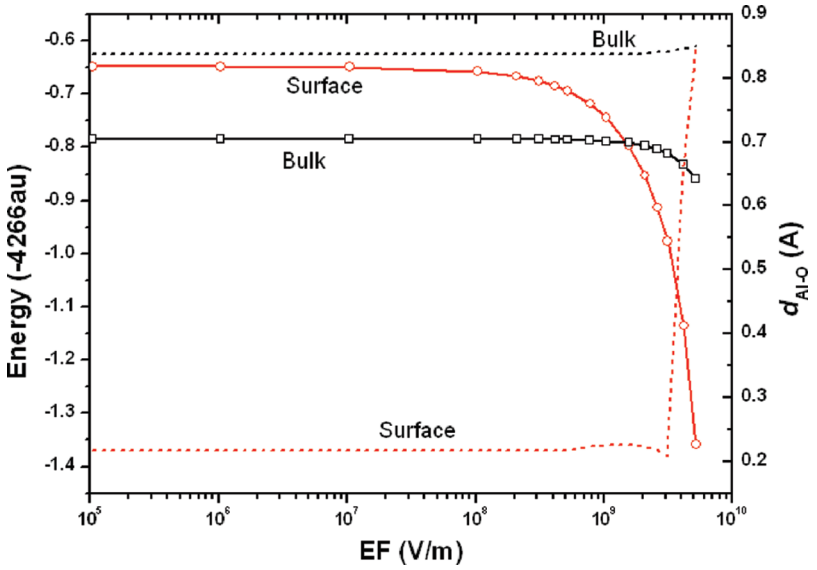

Figure 8. Total electronic energies of the bulk (squares) and the (0001) surface (circles) of the Al_2O_3 unit cell as a function of external electric fields obtained at the BLYP/TNP/5 × 5 × 5 *k*-points level of theory. The Al−O bond of the bulk crystal and the outmost Al_s-O_s bond distances are shown in dashed lines.

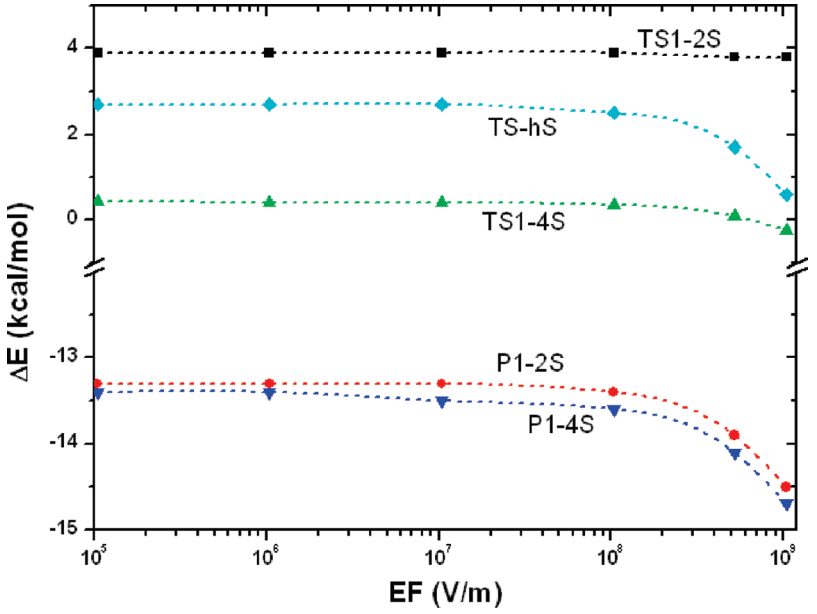

Figure 9. Barrier heights for TS1-2, TS1-4, and TS-h and exothermicities for the formation of P1-2 and P1-4 with respect to the initial adsorption intermediates in the unit-cell models as a function of external electric fields.

theoretical calculation gives the same orders of magnitude for the electric fields. Since the electric fields on high-voltage power lines are usually at 10^6-10^7 V/m order of magnitude, which is still lower than the fields that required to have any significance, it is suggested that the electric fields might play a minor role in the hydroxylation of the $Al_2O_3(0001)$ surface and in the icing of high-voltage power lines.

3.E. Multilayer Water Adsorption/Dissociation. Previously it was stated that the fully hydroxyl covered $Al_2O_3(0001)$ surface resembles a gibbsite-like surface after liberating the top layer of Al as some form of bulk or soluble hydroxide. Therefore, it is interesting to investigate how the second water or more water molecules react with the hydroxylated surface, especially under the high humidity and supercooled conditions of our concern, *before* the top layer of Al is removed.

Starting from the P1-4 structure found in the unit-cell model, one water molecule attacks the surface Al_s atom to form a weakly bonded intermediate Add-2A, as shown in Figure 10. The $Al_s-O_wH_2$ bond is relatively long, 2.231 Å. Meanwhile, the $O-Al_s$ bond increases from 1.731 to 1.849 Å. Water molecule forms two hydrogen bonds with the nearby surface HO group. The distance of one hydrogen bond with water hydrogen as proton donor is only 1.574 Å, significantly shorter than the normal hydrogen bond between H_2O molecules. Vibrational

analysis shows that Add-2A is a true minimum with all real frequencies. However, the binding energy of this adduct is only 1 kcal/mol. With the ZPE correction, it turns out that Add-2A lies 1.3 kcal/mol above the isolated water and P1-4 reactants. The room-temperature free energy ΔG to form Add-2A is as high as 11.6 kcal/mol. Therefore, Add-2A intermediate might not exist under normal conditions.

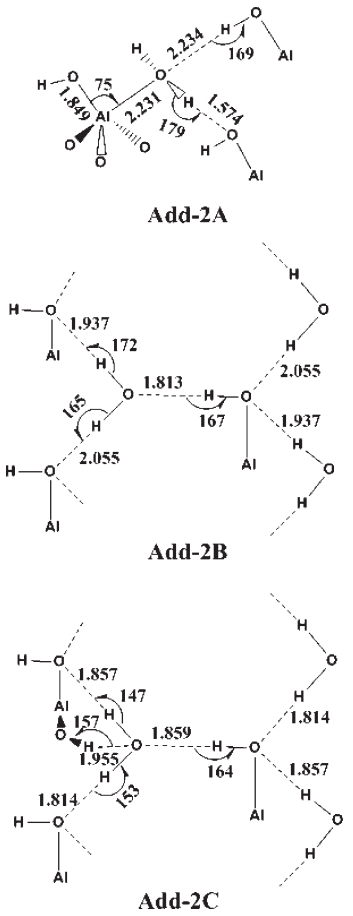

Figure 10. Adsorption intermediates formed by addition of water to the hydroxylated surface. Bond distances are in angstroms, and angles are in degrees.

In order to reveal the kinetic stability of the Add-2A intermediate, partial optimizations by fixing the Al_s-O_w distances and relaxing all other degrees of freedoms were carried out. The minimum energy path for such a dissociation process is shown in Figure 11. Evidently the energy decreases monotonically when the Al_s-O_w bond is stretched and the Al_s-O bond distances decrease to the equilibrium length of the P1-4 species. The resulting structure at the final scanned point corresponds to a hydrogen-bonding complex, Add-2B, as shown in Figure 10. Each water molecule forms three hydrogen bonds with the surface hydroxyl groups, and meanwhile each surface hydroxyl group is surrounded by three water molecules through hydrogen bonds. Therefore, a hexagonal hydrogen-bonded water layer above the alumina plane is produced. The interlayer distance between water O_w and hydroxyl O is 0.94 Å. The binding energy is 16.5 kcal/mol (13.4 kcal/mol with ZPE), which is significantly larger than that of the Add-2A complex.

The above result proves unambiguously that, once the outmost Al_s atom of the (0001) surface is hydroxylated by one H_2O molecule, further hydroxylation of the surface Al_s atom would be very hard to occur. Instead, the water molecule prefers to a form hydrogen-bonding network with the surface hydroxyl groups. While the surface $H-O_s$ group participates in the hydrogen bonding, a slightly more stable complex, denoted as Add-2C, is produced, as shown in Figure 9. The water molecule has to move inward in order to interact with the surface $H-O_s$ with a hydrogen bond of 1.955 Å. The interlayer distance between the water O_w and the hydroxyl O layers decreases to 0.30 Å. The binding energy increases only slightly due to the fourth hydrogen bond in Add-2C, i.e., 17.6 kcal/mol (14.0 kcal/mol with ZPE). Note that the same structure as Add-2C has been found theoretically in the literature.[16]

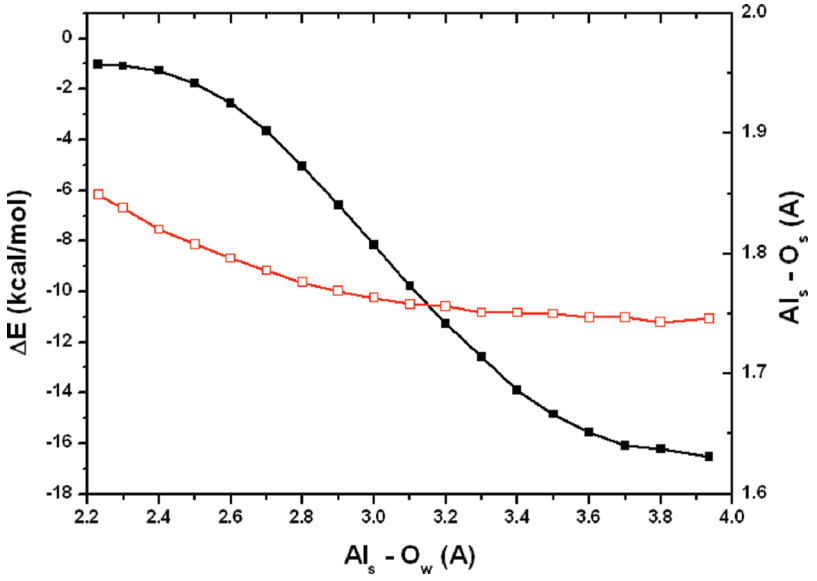

Figure 11. Optimized energies for the stretch of the Al_s-O_w bond starting from the Add-2A intermediate at the BLYP/TNP level. The surface Al_s-O_s bond distances are shown to indicate the restoration of the hydroxylated structure as the water molecule leaves.

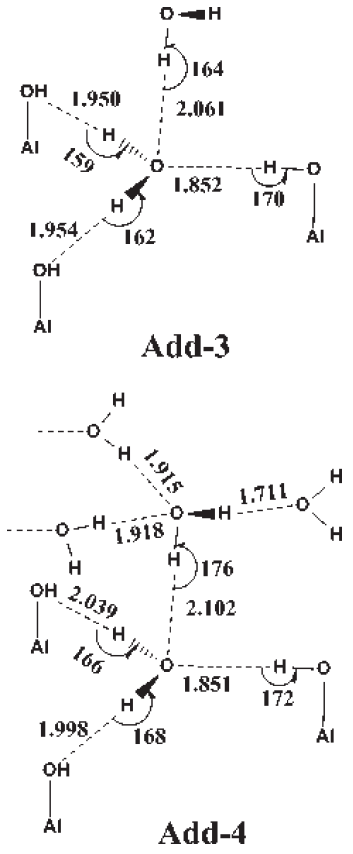

Figure 12. Optimized geometries of the multiple water layers being well arranged on the hydroxylated alumina surface. Bond distances are in angstroms, and angles are in degrees.

It is expected that multiple-layer absorption of water could be generated on the basis of the hexagonal hydrogen-bonded water layers above the alumina plane as illustrated in Figure 10. By adding more water molecules to the hexagonal water layer, the most stable structures for the third layer and the fourth layer of water, denoted as Add-3 and Add-4, respectively, are shown in Figure 12. In fact, there are three possible multiple adsorption configurations for each multiple-layer structure (Figure S1 in the Supporting Information) and only the one with the lowest energies, that is, the most stable configuration among three complexes, is discussed briefly herein. Since the major concern of the present work is the microscopic hydroxylation mechanism of $Al_2O_3(0001)$ surface, more extensive calculations with larger supercells will be reported elsewhere.

For Add-3, the additional water molecule acts as a proton donor to form a hydrogen bond with water molecule. The interlayer distance is 2.76 Å. The structure bonding to the Al_s−OH group does exist but is less stable. The O_w atom of water is pushed backward a little bit as indicated by the decreasing interlayer distance from 0.94 to 0.85 Å. The binding energy of the third water molecule is about 8 kcal/mol (7 kcal/mol with ZPE). For Add-4, the fourth water molecule forms three hydrogen bonds with the outmost water molecule of Add-3 directly. There is nearly no change to the structure of Add-3, and the interlayer distance between the third and the fourth water molecules is 0.70 Å. It is interesting to note that these two new water layers assemble the hexagonal ice 1h structure and the water molecules do fulfill the so-called "ice rule"; that is, each oxygen is covalently bonded to two hydrogen atoms and the oxygen atom in each water molecule forms up to two hydrogen bonds with other oxygens.[34]

Table 4. Vibrational Frequencies for the Multilayer Adsorption Structures of the Hydroxylated $Al_2O_3(0001)$ Surface (in cm^{-1})

species	P1-4	H_2O	Add-2B	Add-2C	Add-3	Add-4
Al_sO−H stretch	3776		3423	3428	3431	3448
O_s−H stretch	3594		3636	3232	3612	3623
W2		3771 (3756)[a]	3511	3361	3454	3428
		3670 (3657)	3287	3290	3338	3342
		1606 (1595)	1637	1586	1640	1641
W3					3728	3531
					3570	3115
					1635	1674
W4						3416
						3407
						1616

[a] Experimental data in parentheses taken from ref 35. Three entries from top to bottom correspond to asymmetrical, symmetrical, and bending modes, respectively.

Further adding water molecules to the unit cell shows that the water molecules prefer to accumulate on the hydroxylated surface through an alternating layer geometry. Vibrational frequencies of the surface hydroxyl groups and those of the absorbed water molecules are listed in Table 4 for comparison. The calculated frequencies for isolated water molecule are in good agreement with the experimental values, an indication of the good quality of the theoretical data. For the hydroxylated surface, the dangling OH stretch is 3776 cm^{-1}, which is nearly the same as that of the isolated water molecule. In contrast, the in-plane O_s−H stretch is only 3594 cm^{-1}, which is 182 cm^{-1} smaller than the upright OH stretch. When water molecules are coordinated to these two surface OH groups, the dangling OH stretch decreases significantly to around 3430 (e.g., 3423−3448) cm^{-1}, that is, is red-shifted by more than 300 cm^{-1}. It is noted that the vibrational mode around 3430 cm^{-1} has not been well established experimentally.[3] However, the present results, together with the results obtained by Ranea, Carmichael, and Schneider,[20] confirm that the mode at 3430 cm^{-1} should be assigned to the perturbed upright Al_s−O−H stretch due to water coordination. The O_s−H stretch is blue-shifted except for the Add-2C complex because the absorbed water molecule forms an additional hydrogen bond with the O_s−H group. In view of the vibrations of water molecules, both asymmetrical and symmetrical O_w−H_w stretch modes are significantly red-shifted by about 400 cm^{-1}, centering in the 3300−3500 cm^{-1} region (e.g., ice-like frequencies). The bending modes of water molecules are rarely affected in the multiple absorption structures.

The above theoretical findings are very promising because they might shed some new light on the microscopic icing mechanism on the Al_2O_3 basal surface. Molecular dynamics simulation is required to clarify such microscopic picture on the basis of the present quantum chemistry data as like the interfacial simulations between water and alumina reported recently by Argyris, Ho, Cole, and Striolo.[36] This part of the work together with the ice accumulation process at the defect surface will be reported in the future.

The effect of electric fields on the structures of the multiple-layer absorption of water on the hydroxylated Al_2O_3 surface has been examined as well. For the electric fields of concern in the ice accretion on high-voltage overhead power lines, that is, $0-10^7$ V/m, there is no observable change in either structural parameters or binding energies for all the complexes considered in this work. It is conceivable that electric fields might not play an important role in the hdyroxylation and subsequent water adsorption process unless the fields increase to 10^9 V/m and above.

3.F. Error Analysis. The present work represents the first theoretical study of the hydrolysis mechanism of the α-Al_2O_3-(0001) surface using the first-principles all-electron basis sets. It is interesting to check the accuracy of such a methodology on both structure and energetics especially for those hydrogen-bonding structures involved in this work.

In our slab models, the vacuum regions between slabs have been used to avoid unphysical interaction. The vacuum thickness was always set to be 10 Å for the α-Al_2O_3(0001) surface. When water molecules are presented on the surface, e.g., for those multiple-layer water absorption structures, the vacuum thickness has been extended to ensure that the unphysical interaction is negligible. For example, for the initial water absorbed intermediate (Add-1), when larger vacuum regions are employed, the changes of total electronic energies are less than 0.01 kcal/mol and the binding energy decreases by only about 1% (see Table S1 in the Supporting Information).

The exchange-correlation BLYP functional was employed for first-principles calculations in our work. There is no particular reason for the choice of this functional at first thought since the same functional has been used in previous work and thus it is convenient for comparison.[18,19] However, the use of this functional has been justified in comparison with the use of other functionals such as PW91, PBE, and HCTH.[37−39] The energetic reaction routes for the unit-cell model as shown in Figure 2 were recalculated with the TNP basis set and $3 \times 3 \times 3$ k-point mesh. The structural parameters and the energetics are compared in Figure S2 and Table S2 in the Supporting Information, respectively. There are no significant differences in the key bond lengths and angles for complexes and transition states. Although the binding energy of Add-1 depends on the functionals, for instance, 28 kcal/mol by PW91 to 21.7 kcal/mol by HCTH, the barrier heights for the subsequent dissociation channels appear to be less sensitive to the functionals. More interestingly, the structural parameters and energies obtained by BLYP appear to be in the middle of those by the other three functionals. On the other hand, the surface relaxation of α-Al_2O_3(0001) has been examined as well, and the results are listed in Table S3 in the Supporting Information. It is evident that PW91, PBE, and HCTH give significantly flatter surface structures than BLYP. Although the surface energies obtained by all the functionals are very close to each other, the relaxation ratio obtained by BLYP is in the best agreement with the experimental value. Therefore, the BLYP functional should be an appropriate method for the mechanistic study of surface reactions of our concern.

The performance of various functionals on the multiple-layer water absorption complexes has been checked by optimization of the structure of the complex Add-2C. The results are shown in Figure S3 in the Supporting Information. Apparently, the lengths of hydrogen bonds show strong dependence on the functionals, especially the hydrogen bond between oxygen of water and hydrogen of the surface O_sH group. Both PW91 and PBE predict much shorter hydrogen bonds than HCTH, while the BLYP method gives a value in the middle. In the case of the binding energy, both PW91 and PBE predict the strongest binding while HCTH results in the weakest binding. Therefore, BLYP appears to be more appropriate than other functionals.

A well-known deficiency in DFT lies in the fact that normally it does not work well for weak interactions. Because many hydrogen-bonding interactions exist for the species involved in this work, especially the multiple-layer water adsorption structures, it is worth investigating how well the present BLYP/TNP method performs on the hydrogen bond. Note that previously it was shown that the DFT/TNP method outperforms Gaussian-based methods in the prediction of structural parameters and binding energies for various hydrogen-bonding complexes and Al_n clusters.[25−27]

First, the $(H_2O)_{n=1-7,20}$ clusters were calculated using the BLYP/TNP method. The geometries and binding energies are summarized in Figure S4 and Table S4 in the Supporting Information, respectively. For comparison, a long-range corrected hybrid density functional with damped dispersion corrections, termed wB97XD,[40] has been employed in the calculations with the smaller 6-31+G(d,p) and the larger 6-311++G(3df,3pd) basis sets, respectively. As shown in Figure S4 and Table S4 in the Supporting Information, the BLYP/TNP is significantly superior for both bonded and nonbonded interactions. The structural parameters and energies obtained by BLYP/TNP are similar to those at the wB97XD/6-311++G(3df,3pd) level of theory and much better. For the $(H_2O)_2$ cluster, the BLYP/TNP method outperforms all other methods including MP2 at the complete basis set limit in view of the OO distance and the binding energy.[41] It is worth noting that the BLYP/TNP calculated binding energy for $(H_2O)_2$ is nearly the same as the most recent quantum Monte Carlo calculation.[42]

Second, in order to mimic the water/Al_2O_3(0001) absorption structures in the periodic slab model, the hydrolysis of Al_4O_6 cluster and the hydrogen-bonding clusters between H_2O and $Al_4O_7H_2$ were investigated using both BLYP/TNP and wB97XD methods. The geometries of various water adsorption clusters are shown in Figure S5 in the Supporting Information, and the energies are summarized in Table S5 in the Supporting Information for comparison. Evidently, the BLYP/TNP calculated data are very close to those obtained at the wB97XD/6-311++G-(3df,3pd) level of theory. Normally the lengths of hydrogen bonds differ by less than 0.02 Å and the binding energies differ by less than 1 kcal/mol for water molecular complexes with up to four H_2O molecules. Therefore, it should be reasonable to conclude that the BLYP/TNP method is able to give reliable water adsorption structures and energetics within chemical accuracy.

Third, the vibrational frequencies of various water clusters and $Al_4O_7H_2-(H_2O)_n$ clusters calculated using both BLYP/TNP and wB97XD/6-311++G(3df,3pd) are summarized in Table S6 in the Supporting Information for comparison. A reasonable agreement between these two sets of methods could be observed. Moreover, the calculated zero-point energies at the BLYP/TNP level are generally lower than those at the wB97XD/6-311++G(3df,3pd) level. It is well-known that the vibrational frequencies and ZPE obtained by Gaussian-based methods are overestimated in comparison with the experimental data. Therefore, the BLYP/TNP calculated frequencies and zero-point energies could be in better agreement with the experimental data.

Finally, the performance of BLYP/TNP was checked by optimizing the structure of ice 1h. Using various ice 1h models

available in previous work,[43,44] the unit cell of ice 1h was fully optimized and the results are listed in Figure S6 in the Supporting Information. The calculated OO distances in different models are all in agreement with the experimental data. The lattice energy was estimated to be 14.5 kcal/mol, which is somewhat higher than the experimental value of 13.4 kcal/mol.[45] It is noteworthy that the BLYP/TNP method is able to predict much better ice density than force-field-based simulations.[44]

All the above analysis should give us confidence that the present all-electron BLYP slab modeling of the surface chemical reactions and water adsorption mechanisms on the α-Al_2O_3-(0001) is reliable in terms of both structure and energetics. While some good agreements with previous theoretical simulations and experimental observations concerning surface relaxation and reaction mechanism have been obtained, further experiments on the kinetics of hydrolysis and on the multiple-layer absorption structures are desired to assess the present theoretical predictions.

4. CONCLUSIONS

Microscopic mechanisms for the reactions of water molecules with the Al_2O_3(0001) surface have been investigated using the density functional theory (BLYP) with the all-electron triple numerical basis sets with polarization and the converged *k*-point mesh. The unit-cell model and the 2 × 2 supercell model were employed to simulate the water coverage. It was found that the adsorption of water on the surface is in the molecular form. The subsequent dissociation occurs via either 1,2- or 1,4-hydrogen migration transition states. While the barrier to the 1,4-reaction path is always lower than that to the 1,2-reaction path, the two channels are competitive and the hydroxylation prefers to occur at the surface Al site and the nearest surface O site. The formation of hydroxylated products is highly exothermic. The surface hydrogen atom is capable of roaming around the surface oxygen atoms.

Electric fields might not play any significant role in the surface reconstruction of Al_2O_3 or in the surface hydroxylation. However, extremely high electric fields above 10^9 V/m might lead the basal surface of Al_2O_3 to change rapidly to the bulk-like structure and result in negative surface energy. Moreover, the presence of strong electric fields will lower the barrier to dissociation and increase the exothermicity.

It is confirmed that the fully hydroxylated Al_2O_3(0001) surface is relatively inert to further hydroxylation. Water molecules prefer to form multiple adsorbed layers through hydrogen-bonding interactions with the hydroxylated surface rather than continuously hydroxylate the surface Al atom. It is predicted that the layered hexagonal ice 1h structure could be formed on the basis of the fully hydoxylated Al_2O_3(0001) surface.

■ ASSOCIATED CONTENT

Ⓢ Supporting Information. Three-dimensional structural visualization of multiple layer complexes and the extensive assessment of the BLYP/TNP method for hydrogen-bonding species. This material is available free of charge via the Internet at http://pubs.acs.org.

■ AUTHOR INFORMATION

Corresponding Author

*E-mail: baoshan@whu.edu.cn. Phone: (86)27-6875-6347.

■ ACKNOWLEDGMENT

Financial support was provided, in part, by the Key Projects in the National Science & Technology Pillar Program during the Eleventh Five-Year Plan Period (No. 2009BAA23B01-1-A). The authors thank the two anonymous referees for their very helpful comments.

■ REFERENCES

(1) Farzaneh, M. Ice accretions on high-voltage conductors and insulators and related phenomena. *Philos. Trans.: Math. Phys. Eng. Sci.* **2000**, *358* (1776), 2971–3005.

(2) Coustet, V.; Jupille, J. High-resolution electron-energy-loss spectroscopy of isolated hydroxyl-groups on α-Al_2O_3(0001). *Surf. Sci.* **1994**, *309* (2), 1161–1165.

(3) Zhang, L.; Tian, C.; Waychunas, G. A.; Shen, Y. R. Structures and charging of α-alumina(0001)/water interfaces studied by sum-frequency vibrational spectroscopy. *J. Am. Chem. Soc.* **2008**, *130* (24), 7686–7694.

(4) Elam, J. W.; Nelson, C. E.; Cameron, M. A.; Tolbert, M. A.; George, S. M. Adsorption of H_2O on a single-crystal α-Al_2O_3(0001) surface. *J. Phys. Chem. B* **1998**, *102* (36), 7008–7015.

(5) Nelson, C. E.; Elam, J. W.; Cameron, M. A.; Tolbert, M. A.; George, S. M. Desorption of H_2O from a hydroxylated single-crystal α-Al_2O_3(0001) surface. *Surf. Sci.* **1998**, *416* (3), 341–353.

(6) Gan, Y.; Franks, G. V. High resolution AFM images of the α-Al_2O_3 single crystal (0001) surface in water. *J. Phys. Chem. B* **2005**, *109* (25), 12474–12479.

(7) Barth, C.; Reichling, M. Imaging the atomic arrangements on the high-temperature reconstructed α-Al_2O_3(0001) surface. *Nature* **2001**, *414*, 54–57.

(8) Eng, P. J.; Trainor, T. P.; Brown, G. E.; Waychunas, G. A.; Newville, M.; Sutton, S. R.; Rivers, M. L. Structure of the hydrated α-Al_2O_3 (0001). *Surf. Sci.* **2000**, *288* (5468), 1029–1033.

(9) Ranea, V. A.; Schneider, W. F.; Carmichael, I. DFT characterization of coverage dependent molecular water adsorption modes on α-Al_2O_3(0001). *Surf. Sci.* **2008**, *602* (1), 268–275.

(10) Polly, R.; Schimmelpfennig, B.; Florsheimer, M.; Kruse, K.; Monem, A.; Klenze, R.; Rauhut, G.; Fanghanel, T. Theoretical investigation of the water/corundum(0001) interface. *J. Chem. Phys.* **2009**, *130* (6), 064702.

(11) Fernandez, E. M.; Eglitis, R.; Borstel, G.; Balbas, L. C. Ab initio calculations of H_2O and O_2 adsorption on Al_2O_3 substrates. *Comput. Mater. Sci.* **2007**, *39* (3), 587–592.

(12) Wang, X. G.; Chaka, A.; Schefer, M. Effect of the environment on α-Al_2O_3 (0001) surface structures. *Phys. Rev. Lett.* **2000**, *84* (16), 3650–3653.

(13) Shapovalov, V.; Truong, T. N. Ab initio study of water adsorption on α-Al_2O_3(0001) crystal surface. *J. Phys. Chem. B* **2000**, *104* (42), 9859–9863.

(14) Lodziana, Z.; Norskov, J. K.; Stoltze, P. The stability of the hydroxylated (0001) surface of α-Al_2O_3. *J. Chem. Phys.* **2003**, *118* (24), 11179–11188.

(15) de Leeuw, N. H.; Parker, S. C. Effect of chemisorption and physisorption of water on the surface structure and stability of α-alumina. *J. Am. Ceram. Soc.* **1999**, *82* (11), 3209–3216.

(16) Thissen, P.; Grundmeier, G.; Wippermann, S.; Schmidt, W. G. Water adsorption on the α-Al_2O_3(0001) surface. *Phys. Rev. B* **2009**, *80* (24), 245403.

(17) Wittbrodt, J. M.; Hase, W. L.; Schlegel, H. B. Ab initio study of the interaction of water with cluster models of the aluminum terminated (0001) α-aluminum oxide surface. *J. Phys. Chem. B* **1998**, *102* (34), 6539–6548.

(18) Hass, K. C.; Schneider, W. F.; Curioni, A.; Andreoni, W. The chemistry of water on alumina surfaces: reaction dynamics from first principles. *Science* **1998**, *282* (5387), 265–268.

(19) Hass, K. C.; Schneider, W. F.; Curioni, A.; Andreoni, W. First-principles molecular dynamics simulations of H_2O on α-Al_2O_3(0001). *J. Phys. Chem. B* **2000**, *104* (23), 5527–5540.

(20) Ranea, V. A.; Carmichael, I.; Schneider, W. F. DFT investigation of intermediate steps in the hydrolysis of α-Al_2O_3(0001). *J. Phys. Chem. C* **2009**, *113* (6), 2149–2158.

(21) Delley, B. From molecules to solids with the DMol^3 approach. *J. Chem. Phys.* **2000**, *113* (18), 7756–7764.

(22) Becke, A. D. A multicenter numerical integration scheme for polyatomic molecules. *J. Chem. Phys.* **1998**, *88* (4), 2547–2553.

(23) Lee, C.; Yang, W.; Parr, R. G. Development of the Colle-Salvtti correlation-energy formula into a functional of the electron density. *Phys. Rev. B* **1998**, *37* (2), 786–789.

(24) Gill, P. M. W.; Johnson, B. G.; Pople, J. A.; Frisch, M. J. An investigation of the performance of a hybrid of Hartree-Fock and density functional theory. *Int. J. Quantum Chem.* **1992**, *44* (S26), 319–331.

(25) Inada, Y.; Orita, H. Efficiency of numerical basis sets for predicting the binding energies of hydrogen bonded complexes: evidence of small basis set superposition error compared to Gaussian basis sets. *J. Comput. Chem.* **2008**, *29* (2), 225–232.

(26) Fowler, J. E.; Ugalde, J. M. Al_{12} and the Al@Al_{12} clusters. *Phys. Rev. A* **1998**, *58* (1), 383–388.

(27) Henry, D. J.; Varano, A.; Yarovsky, I. Performance of numerical basis set DFT for aluminum clusters. *J. Phys. Chem. A* **2008**, *112* (40), 9835–9844.

(28) Guenard, P.; Renaud, G.; Barbier, A.; Gautier-Soyer, M. Determination of the α-Al_2O_3(0001) surface relaxation and termination by measurements of crystal truncation rods. *Surf. Rev. Lett.* **1998**, *5* (1), 321–324.

(29) Ahn, J.; Rabalais, J. W. Composition and structure of the Al_2O_3{0001}-(1 $\times$ 1) surface. *Surf. Sci.* **1997**, *388* (1/3), 121–131.

(30) McHale, J. M.; Navrotsky, A.; Perrotta, A. J. Effects of increased surface area and chemisorbed H_2O on the relative stability of nanocrystalline γ-Al_2O_3 and α-Al_2O_3. *J. Phys. Chem. B* **1997**, *101* (4), 603–613.

(31) McHale, J. M.; Auroux, A.; Perrotta, A. J.; Navrotsky, A. Surface energies and thermodynamic phase stability in nanocrystalline aluminas. *Science* **1997**, *277*, 788–791.

(32) Johnston, H. S.; Heickle, J. Tunneling corrections for unsymmetrical Eckart potential energy barriers. *J. Phys. Chem.* **1962**, *66* (3), 532–533.

(33) Stan, C. A.; Tang, S. K. Y.; Bishop, K. J. M.; Whitesides, G. M. Externally applied electric fields up to 1.6 $\times$ 10^5 V/m do not affect the homogeneous nucleation of ice in supercooled water. *J. Phys. Chem. B* **2011**, *115* (5), 1089–1097.

(34) Bernal, J. D.; Fowler, R. H. A theory of water and ionic solution, with particular reference to hydrogen and hydroxyl ions. *J. Chem. Phys.* **1933**, *1* (8), 515–548.

(35) Shimanouchi, T. Tables of molecular vibrational frequencies, consolidated volume I. *Natl. Stand. Ref. Data Ser. (U. S., Natl. Bur. Stand.)* **1972**, *NRSDS-NBS 39*, 1–160.

(36) Argyris, D.; Ho, T.; Cole, D. R.; Striolo, A. Molecular dynamics studies of interfacial water at the alumina surface. *J. Phys. Chem. C* **2011**, *115* (5), 2038–2046.

(37) Perdew, J. P.; Wang, Y. Accurate and simple analytic representation of the electron-gas correlation energy. *Phys. Rev. B* **1992**, *45* (23), 13244–13249.

(38) Perdew, J. P.; Burke, K.; Ernzerhof, M. Generalized gradient approximation made simple. *Phys. Rev. Lett.* **1996**, *77* (18), 3865–3868.

(39) Boese, A. D.; Handy, N. C. A new parametrization of exchange-correlation generalized gradient approximation functionals. *J. Chem. Phys.* **2001**, *114* (13), 5497–5503.

(40) Chai, J. D.; Head-Gordon, M. Long-range corrected hybrid density functionals with damped atom−atom dispersion corrections. *Phys. Chem. Chem. Phys.* **2008**, *10*, 6615–6620.

(41) Santra, B.; Michaelides, A.; Scheffler, M. On the accuracy of density-functional theory exchange-correlation functionals for H bonds in small water clusters: Benchmarks approaching the complete basis set limit. *J. Chem. Phys.* **2007**, *127* (18), 184104–1/8.

(42) Benedek, N. A.; Snook, I. K.; Towler, M. D.; Needs, R. J. Quantum Monte Carlo calculations of the dissociation energy of the water dimer. *J. Chem. Phys.* **2006**, *125* (10), No. 104302-1/5.

(43) Morrison, I.; Li, J.-C.; Jenkins, S.; Xantheas, S. S.; Payne, M. C. Ab-initio total energy studies of the static and dynamical properties of ice 1h. *J. Phys. Chem. B* **1997**, *101* (32), 6146–6150.

(44) Hammer, S. M.; Panisch, R.; Kobus, M.; Glinnemanna, J.; Schmidt, M. U. Simulation of absorption sites of acetone at ice: (0001) surface, bulk ice and small-angle grain boundaries. *CrystEngComm* **2009**, *11*, 1291–1302.

(45) Hermann, A.; Schwerdtfeger, P. Ground-state properties of crystalline ice from periodic Hartree-Fock calculations and a coupled-cluster-based many-body decomposition of the correlation energy. *Phys. Rev. Lett.* **2008**, *101* (18), No. 183005-1/4.

(46) McQuarrie, D. A.; Simon, J. D. *Physical Chemistry, a Molecular Approach*; University Science Books: Sausalito, CA, USA, 1997.